Manuscript submitted to
AIMS' Journals
Volume **X**, Number **0X**, XX **200X**

Website: http://AIMsciences.org

pp. **X–XX**

THE ROLE OF PROCESSING SPEED IN DETERMINING STEP PATTERNS DURING DIRECTIONAL EPITAXY

Michael A. Saum

Department of Mathematics, University of Tennessee
Knoxville, TN, 37996, USA

Tim P. Schulze

Department of Mathematics, University of Tennessee
Knoxville, TN, 37996, USA

(Communicated by the associate editor name)

Abstract. We consider the growth of an epitaxial thin film on a continuously supplied substrate using both the Burton-Cabrara-Frank (BCF) mean-field model and kinetic Monte-Carlo (KMC) simulation. Of particular interest are effects due to the finite size of the deposition zone, which is modeled by imposing an up- and downwind adatom density equal to the adatom density on an infinite terrace in equilibrium with a step. For the BCF model, we find this scenario admits a steady-state pattern with a specific number of steps separated by alternating widths. The specific spacing between the steps depends sensitively on the processing speed and on whether the number of steps is odd or even, with the range of velocities admitting an odd number of steps typically much narrower. These predictions are only partially confirmed by KMC simulations, however, with particularly poor agreement for an odd number of steps. To investigate further, we consider alternative KMC simulations with the interactions between random walkers on the terraces neglected so as to conform more closely with the mean field model. The latter simulations also more readily allow one to disable the step detachment mechanism, in which case they agree well with the predictions of the BCF model.

1. **Introduction.** The epitaxial growth of thin films is an increasingly sophisticated and much studied process where one or more layers of crystalline material are deposited on an existing crystal. As demand for the resulting materials grows it seems likely that the means by which the films are produced will gradually shift from batch to continuous processing, where substrate in the form of wire or tape is continuously pulled through a fixed deposition zone (Fig. 1). For example, continuous processing is currently used to produce large quantities of superconducting wire [3, 5, 12]. It is natural to consider this process, which has previously been referred to as *reel-to-reel processing* or *directional epitaxy* [9], in the laboratory frame of reference, where the mean surface morphology achieves a steady-state. In the context of most existing analysis and simulation of epitaxial growth—which assumes an infinitely extended substrate, some form of periodic boundary conditions, and a

2000 *Mathematics Subject Classification.* Primary: 82B80, 82B21; Secondary: 82D25,65C05.
Key words and phrases. Epitaxial Growth, Kinetic Monte Carlo, Continuous Processing.
This work was supported by grants from DOE (DE-FG02-03ER2558) and NSF (NSF-DMS-0707443).

quasistatic approximation—bulk motion of the film plays no role. When one considers finite size effects, however, we show that the motion of the film relative to the boundaries of the deposition zone can significantly affect surface patterns. These effects will be especially pronounced for small deposition zones or within boundary layers near the ends of larger deposition zones.

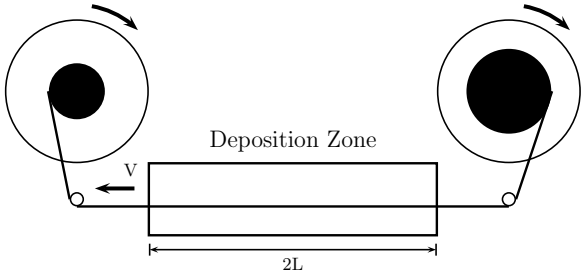

FIGURE 1. Sketch of Reel-to-Reel Processing System (side view). The substrate is being pulled to the left with velocity V and moves through a fixed deposition zone of length $2L$ while being exposed to a uniform deposition flux F. In a steady (or approximately steady) state, this flux will drive the surface morphology to the right, relative to the film, at a rate that matches the pulling velocity, leaving it stationary (or approximately stationary) in the laboratory frame of reference.

Mathematical models of epitaxial films have taken many forms. We shall consider two of the more common approaches—a mean field approach, referred to as the Burton-Cabrera-Frank (BCF) model, and a Markov chain approach, referred to as kinetic Monte Carlo (KMC). In both of these approaches, the surface of the film is assumed to grow in discrete layers with a thickness that corresponds to a single unit cell, often a single atom, of the crystal. Normally, several layers of growth may be exposed simultaneously and it is the patterns formed by the boundaries of these layers that are of principal interest. Material is added very slowly by various deposition processes, allowing time for it to diffuse to the steps on the surface and incorporate itself into the crystal in a coherent pattern. In KMC, this too is modeled discretely, with atoms arriving one at a time according to some stochastic process and the resulting random walkers are referred to as *adatoms*. In the BCF models, the deposition is treated in an average sense and one tracks only the mean density of adatoms as a piecewise smooth function of position. These models will be introduced more fully in Sections 2 and 3 below. In work closely related to the present study, Schulze [9] has used both types of models to examine the morphological stability and fluctuations of the boundary of a single monolayer of growth during directional epitaxy. We extend this work to study the influence of processing speed in a multi-step scenario, but restrict our analysis to $1+1$ dimensional growth (i.e., a one dimensional surface plus the growth direction.)

More specifically, we study uniform deposition of atoms at rate F on a train of n steps being pulled with a fixed velocity V through a deposition zone of length $2L$. In a steady (or approximately steady) state, this flux will drive the surface morphology to the right, relative to the film, at a rate that matches the pulling velocity, leaving it stationary (or approximately stationary) in the laboratory frame of reference.

Our interest is in finite-size effects, which we model by imposing an equilibrium concentration of adatoms on the up- and down-stream ends of the deposition zone. Our principal observation is that this induces an alternating step-spacing pattern, with two characteristic widths that vary with the pulling velocity. In contrast, one normally only considers uniformly spaced steps in an infinitely extended system.

In Section 2 we begin with the BCF model, determining the allowed steady-states and their linear stability. In Section 3, we introduce the KMC model and corresponding numerical simulations along with modifications to the KMC model to produce simulations that more accurately reflect assumptions inherent to the mean field approach and that, therefore, give much better agreement with the BCF model. We conclude in Section 4.

2. **Mean Field Model.** The BCF [1] model is a mean-field model formulated in terms of an adatom density $\rho_i(x, y, t)$ on each of several discrete terraces $i = 1, 2, \ldots$, separated by steps, which are modeled as continuous, smoothly varying curves in the plane. Typically, the adatom density is small, on the order of 10^{-7}–10^{-5} adatoms per unit area. Despite this fact, the number density approximation has received wide acceptance and seems to offer insight into some pattern formation processes, such as the step-meandering instability [2].

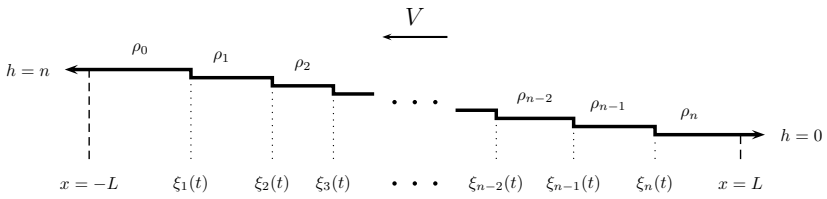

FIGURE 2. Geometry: n steps, $n + 1$ terraces (side view). The steps are descending to the right with their positions measured in the laboratory frame, and the pulling velocity V is in the opposite direction.

Fig. 2 illustrates the basic system geometry we consider. Notice that the positions of the steps are measured in the stationary frame of the deposition zone. Our focus here is on determining steady states of the $1 + 1$ dimensional model. After some simplifications of the $2 + 1$-dimensional model as presented in Schulze [9], we arrive at:

$$\partial_t \rho_j - V \partial_x \rho_j = D \partial_x^2 \rho_j + F, \quad \xi_j < x < \xi_{j+1},\ j = 0, \ldots, n \tag{1}$$

$$\pm D \partial_x \rho \big|_{\pm} \pm (V + \partial_t \xi_j) \rho \big|_{\pm} = k_{\pm} \left(\rho - \rho_e\right) \big|_{\pm}, \quad x = \xi_j(t),\ j = 1, \ldots, n \tag{2}$$

$$\rho_n = \rho_0 = \rho_e, \quad x = \pm L \tag{3}$$

$$\left(\rho_a - [\rho]_-^+\right) (V + \partial_t \xi_j) = D \left[\partial_x \rho\right]_-^+, \quad x = \xi_j(t),\ j = 1, \ldots, n, \tag{4}$$

where ξ_j denotes the position of terrace boundaries, ρ_a is the density of lattice sites on the surface, and V, F, L and n are parameters identified in the introduction. The equilibrium adatom density ρ_e is the expected adatom density on a terrace in equilibrium with a step, a state we take as an approximate model for the up- and down-wind conditions in a continuous processing apparatus. The parameters D and $k_{\pm}$ specify the rate of surface diffusion and attachment rates at the right, k_+, or left, k_-, side of a step. In general, these asymmetric step attachment parameters model

step edge barriers [6, 8, 10]. The case $k_+ > k_-$ leads to the much-studied, two-dimensional meandering instability [2]; the case $k_+ < k_-$ is known to give rise to a step-bunching instability [8, 10], where steps combine to form multi-step boundaries. We take $k_+ = k_- = D$, where D is the adatom terrace diffusion coefficient in the BCF model. Finally, we discard all terms involving step curvature and do not have any terms representing island nucleation, adatom mobility along step edges, or step edge kink effects. We will explore the limitations of these assumptions below.

We use a quasistatic approximation which assumes the adatom density equilibrates fast compared to the motion of the steps. This regime is characterized by small F and V, which then results in small ρ and, once quasiequilibrium has been established, slow variation in time. Accordingly, we neglect terms of second order of smallness in (1)–(4). Rewriting $\rho - \rho_e \longrightarrow \rho$, and scaling lengths so that the lattice spacing $a = 1$ and time so that $D = 1$, we arrive at the following 1-D continuum system:

$$0 = \partial_x^2 \rho_j + F, \quad \xi_j < x < \xi_{j+1},\ j = 0, \dots, n \tag{5}$$

$$\partial_x \rho_j|_+ = \rho_j|_+, \quad \text{at } x = \xi_j,\ j = 1, \dots, n \tag{6}$$

$$-\partial_x \rho_{j-1}|_- = \rho_{j-1}|_-, \quad \text{at } x = \xi_j,\ j = 1, \dots, n \tag{7}$$

$$\rho_n = \rho_0 = 0, \quad \text{at } x = \pm L, \text{ respectively} \tag{8}$$

$$V + \partial_t \xi_j = \partial_x \left(\rho_j - \rho_{j-1}\right), \quad \text{at } x = \xi_j,\ j = 1, \dots, n. \tag{9}$$

To avoid overhanging steps, we require the step positions $\boldsymbol{\xi} \equiv \{\xi_1, \xi_2, \dots, \xi_n\}$ to satisfy

$$-L < \xi_1 < \xi_2 < \cdots < \xi_n < L.$$

Equation (5) admits solutions of the form

$$\rho_j(x,t) = A_j(\boldsymbol{\xi}(t)) + B_j(\boldsymbol{\xi}(t))x - \frac{Fx^2}{2}, \quad j = 0, 1, \dots, n. \tag{10}$$

Substitution of (10) into (5)–(8) gives the algebraic system:

$$\begin{pmatrix} -1 & L & & & & & \\ 1 & 1+\xi_1 & & & & & \\ & & -1 & 1-\xi_1 & & & \\ & & 1 & 1+\xi_2 & & & \\ & & & \ddots & \ddots & & \\ & & & & -1 & 1-\xi_n \\ & & & & 1 & L \end{pmatrix} \begin{pmatrix} A_0 \\ B_0 \\ A_1 \\ B_1 \\ \vdots \\ A_n \\ B_n \end{pmatrix} = \begin{pmatrix} -FL^2/2 \\ F\xi_1 + F\xi_1^2/2 \\ F\xi_1 - F\xi_1^2/2 \\ F\xi_2 + F\xi_2^2/2 \\ \vdots \\ F\xi_n - F\xi_n^2/2 \\ FL^2/2 \end{pmatrix}. \tag{11}$$

Note that for boundary conditions other than Dirichlet (8), such as Neumann or mixed, only the first and last components of the right hand side of (11) need be modified. The block diagonal structure of the system implies that the adatom

density profile coefficients $\{A_j, B_j\}_{j=0}^n$ are given by:

$$A_j = \begin{cases} \dfrac{FL(2\xi_1 + \xi_1^2 + L(1+\xi_1))}{2(1+\xi_1+L)}, & j=0 \\ \dfrac{F(\xi_{j+1} - \xi_j(\xi_{j+1}+1))}{2}, & j=1,\dots,n-1 \\ \dfrac{-FL(2\xi_n - \xi_n^2 + L(\xi_n - 1))}{2(1-\xi_n+L)}, & j=n \end{cases} \tag{12}$$

$$B_j = \begin{cases} \dfrac{F(\xi_1^2 + 2\xi_1 - L^2)}{2(1+\xi_1+L)}, & j=0 \\ \dfrac{F(\xi_j + \xi_{j+1})}{2}, & j=1,\dots,n-1 \\ \dfrac{F(L^2 + 2\xi_n - \xi_n^2)}{2(1-\xi_n+L)}, & j=n. \end{cases} \tag{13}$$

Equation (9) then takes the form of a nonlinear system of ordinary differential equations for the step positions $\boldsymbol{\xi}(t)$:

$$\partial_t \xi_j = B_j(\boldsymbol{\xi}) - B_{j-1}(\boldsymbol{\xi}) - V, \quad j = 1,\dots,n. \tag{14}$$

2.1. **Steady State Behavior.** We seek steady-state solutions of (14) by setting $\partial_t \xi_j = 0$, giving

$$B_j(\boldsymbol{\xi}) - B_{j-1}(\boldsymbol{\xi}) - V = 0, \quad j = 1,\dots,n. \tag{15}$$

Equation (15) admits solutions of the form:

$$\xi_j = \begin{cases} -L + \delta_L + \dfrac{j}{2}\delta_0 + \left(\dfrac{j}{2} - 1\right)\delta_1, & j \text{ even} \\ -L + \delta_L + \dfrac{j-1}{2}\delta_0 + \dfrac{j-1}{2}\delta_1, & j \text{ odd} \end{cases} \qquad j = 1,\dots,n. \tag{16}$$

We refer to this Ansatz as a *pairwise step pattern (PSP)*, illustrated in Fig. 3 for $n = 6$. Note that the step-widths (δ_0, δ_1) repeat throughout the interior of the domain, and that when $\delta_0 = \delta_1$, one has equidistant step spacing, neglecting the boundary terrace widths. In addition the following global constraint must be satisfied:

$$2L = \begin{cases} \delta_L + \dfrac{n}{2}\delta_0 + \left(\dfrac{n}{2} - 1\right)\delta_1 + \delta_R, & n \text{ even} \\ \delta_L + \dfrac{n-1}{2}\delta_0 + \dfrac{n-1}{2}\delta_1 + \delta_R, & n \text{ odd}. \end{cases} \tag{17}$$

Intuition suggests that PSP's can be explained qualitatively as follows. In the case of symmetric attachment parameters, $k_+ = k_-$, half of the atoms deposited on each terrace will attach to the forward/backward step edge. The speed of a step is therefore proportional to one half the sum of the lengths of the terraces on either side. For all steps to have the same speed, the interior terraces must either all have the same size or alternate in size. The boundary terraces have somewhat different boundary conditions and therefore need not conform to this pattern.

Using (13) and (15) gives the following equations for the step positions $\boldsymbol{\xi}$ ($n \geq 3$):

$$V = \begin{cases} \dfrac{F}{2}\left[\dfrac{(\xi_2 - \xi_1) + (\xi_1 + \xi_2)L + \xi_1\xi_2 + L^2}{1 + L + \xi_1}\right], & j = 1 \\ \dfrac{F}{2}\left(\xi_{j+1} - \xi_{j-1}\right), & j = 2,\dots,n-1 \\ \dfrac{F}{2}\left[\dfrac{(\xi_n - \xi_{n-1}) - (\xi_{n-1} + \xi_n)L + \xi_{n-1}\xi_n + L^2}{1 + L - \xi_n}\right], & j = n. \end{cases} \tag{18}$$

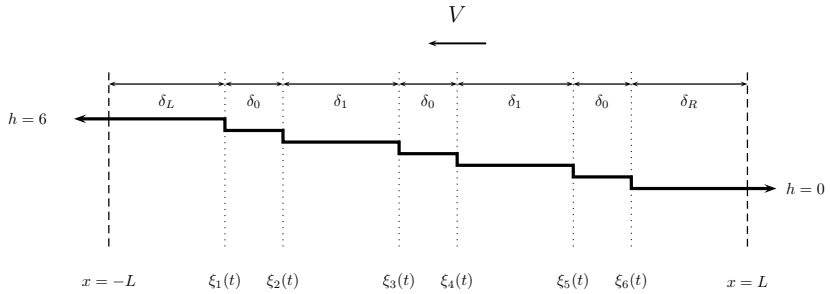

FIGURE 3. Pairwise Step Pattern for $n = 6$. Interior terrace widths appear in an alternating fashion.

For n **odd**, substituting (16) into (18) gives

$$V = \begin{cases} \dfrac{F}{2}\left(\dfrac{\delta_L^2}{\delta_L + 1} + \delta_0\right), & j = 1 \\ \dfrac{F}{2}\left(\delta_0 + \delta_1\right), & j = 2, \ldots, n-1 \\ \dfrac{F}{2}\left(\dfrac{\delta_R^2}{\delta_R + 1} + \delta_1\right), & j = n. \end{cases} \tag{19}$$

For n **even**, $\delta_L = \delta_R$ (due to symmetry), and substituting (16) into (18) gives

$$V = \begin{cases} \dfrac{F}{2}\left(\dfrac{\delta_L^2}{\delta_L + 1} + \delta_0\right), & j = 1, n \\ \dfrac{F}{2}\left(\delta_0 + \delta_1\right), & j = 2, \ldots, n-1. \end{cases} \tag{20}$$

Following the same procedure for $n = 1$ one obtains

$$V = \frac{F}{2}\left(\frac{\delta_L^2}{1 + \delta_L} + \frac{\delta_R^2}{1 + \delta_R}\right), \tag{21}$$

and for $n = 2$ one obtains

$$V = \frac{F}{2}\left(\frac{\delta_L^2}{1 + \delta_L} + \delta_0\right), \quad j = 1, 2. \tag{22}$$

These conditions place constraints on the step positions (or, equivalently the step spacings) by forcing all of the steps to move, relative to the substrate, at a velocity that matches the pulling velocity V.

Solving (19) one obtains for n **odd**

$$\delta_1 = \frac{\delta_L^2}{\delta_L + 1}, \tag{23}$$

$$\delta_0 = \frac{\delta_R^2}{\delta_R + 1}, \tag{24}$$

and solving (20) for n **even**

$$\delta_1 = \frac{\delta_L^2}{\delta_L + 1}. \tag{25}$$

One obtains via telescoping sum of (15) that

$$V = \frac{B_n - B_0}{n}. \tag{26}$$

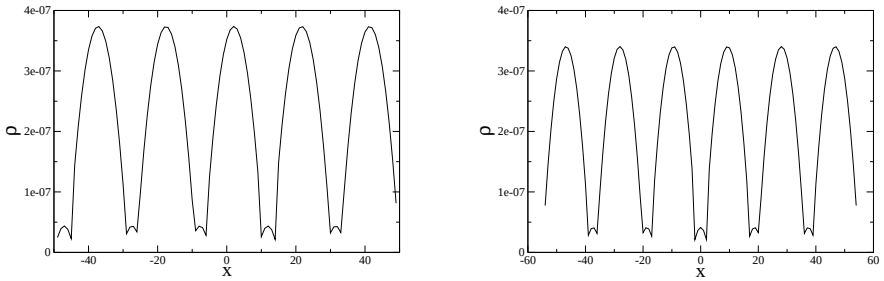

(a) $n = 9$ (odd) (b) $n = 10$ (even)

FIGURE 4. Steady-state adatom density profiles $\rho(x)$. Cusps form at step locations, and the height of the steps (not illustrated) increases from right to left.

This equation is important in that it clearly identifies the relationship between the number of steps n, the pulling velocity V, and the adatom densities on the boundary terraces that must be satisfied for steady-state solutions.

Two examples of steady-state adatom density distributions exhibiting PSP's are shown in Fig. 4. Note the existence of PSP's for both n odd and n even and that the cusps form at step locations while the step heights (not shown) are decreasing to the right.

The differences between n even and n odd for systems exhibiting PSP's are illustrated in Fig. 5. When n is even, steady-state solutions exist for a wide range of velocities, while for n odd steady-state solutions exist over a very narrow range of velocities. In addition, for n even there is only one steady-state solution for each V while for n odd there exist two steady-state solutions for each V.

2.2. **Non Steady Behavior.** For a single step, the ODE for the step position ξ is

$$\partial_t \xi = \frac{F}{2}\left(\frac{(L+\xi)^2}{1+L+\xi} + \frac{(L-\xi)^2}{1+L-\xi}\right) - V. \tag{27}$$

Analysis leads to identification of two equilibrium points $(V^*, \bar{\xi}_1)$, $(V^*, \bar{\xi}_2)$ where

$$\bar{\xi}_{1,2} = \pm\frac{\sqrt{(FL-F-V)(L+1)(FL^2-VL-V)}}{FL-F-V}. \tag{28}$$

These equilibrium points can be expressed in terms of δ_R as $(V^*, \delta_{R,1})$ and $(V^*, \delta_{R,2})$ via the formula $\delta_R = L - \xi$. The stability characteristics of these equilibrium points are illustrated in Fig. 6.

For the single-step case, the stability of the two solution branches can be understood intuitively from the following argument. Due to the quasistatic evolution of the adatom density, the δ_R–V curve will give, to a good approximation, the velocity of a step relative to the substrate when the step is positioned a distance δ_R from the right boundary. As the system slowly evolves toward steady state, the velocity of the step approaches the pulling velocity V. Suppose the initial δ_R is perturbed above the upper branch; the corresponding step velocity will then be faster than the pulling velocity and this will tend to decrease δ_R, moving the system toward steady

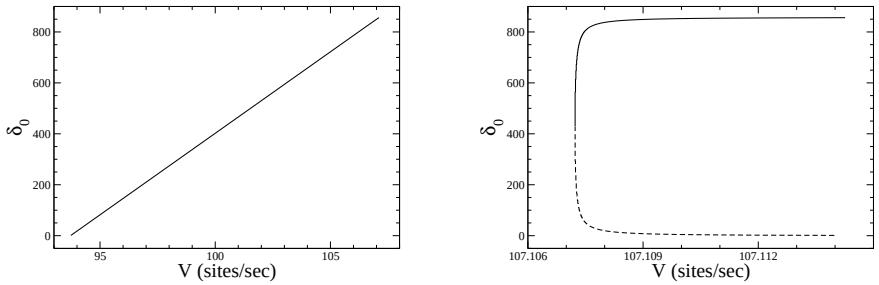

(a) $\delta_0(V)$, $n = 14$ (even) (b) $\delta_0(V)$, $n = 13$ (odd)

FIGURE 5. $\delta_0(V)$ relation in the 1-D BCF continuum model with $F = 0.25$, $2L = 6000$. The range of velocities V for steady-states, the number of steady-state solutions, and the stability characteristics of the steady-state solutions depend on whether the number of steps n is odd or even. Note that for n odd, the upper branch (solid line) is stable and the lower branch (dashed line) is unstable.

state as indicated by the topmost arrow. A similar analysis reveals the direction of the three remaining arrows and indicates that the top branch is stable, while the bottom branch is unstable. This pattern is repeated for larger, odd numbers of steps and this qualitative argument is supported by the following linear stability calculations.

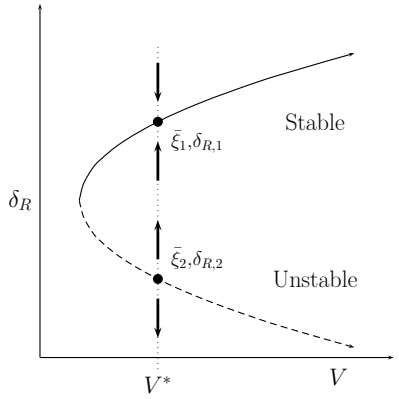

FIGURE 6. Stability diagram for $n = 1$.

The ODE's for $n \geq 3$ step positions $\boldsymbol{\xi}$ can be written as:

$$\partial_t \boldsymbol{\xi} = \partial_t \begin{pmatrix} \xi_1 \\ \xi_2 \\ \vdots \\ \xi_{n-1} \\ \xi_n \end{pmatrix} = \begin{pmatrix} \dfrac{F\left(L^2 + (\xi_1+\xi_2)L + \xi_1\xi_2 + \xi_2 - \xi_1\right)}{2(L+1+\xi_1)} - V \\ \dfrac{F(\xi_3 - \xi_1)}{2} - V \\ \vdots \\ \dfrac{F(\xi_n - \xi_{n-2})}{2} - V \\ \dfrac{-F\left(L^2 - (\xi_{n-1}+\xi_n)L + \xi_{n-1}\xi_n + \xi_n - \xi_{n-1}\right)}{2(-L-1+\xi_n)} - V \end{pmatrix}. \tag{29}$$

The jacobian of the ODE system is thus the tridiagonal matrix:

$$\begin{pmatrix} \dfrac{-F}{2(L+1+\xi_1)^2} & F/2 & & & \\ -F/2 & 0 & F/2 & & \\ & \ddots & \ddots & & \\ & -F/2 & 0 & F/2 & \\ & & -F/2 & \dfrac{F}{2(-L-1+\xi_n)^2} \end{pmatrix}$$

$$= \frac{F}{2} \begin{pmatrix} -(\delta_L+1)^{-2} & 1 & & & \\ -1 & 0 & 1 & & \\ & \ddots & \ddots & & \\ & -1 & 0 & 1 & \\ & & -1 & (\delta_R+1)^{-2} \end{pmatrix}. \tag{30}$$

Referring to Fig. 5 (see also Figs. 8,9), one can show that for n even, steady-states exist for a wide range of velocities, and the Jacobian evaluated at the valid fixed points has purely imaginary eigenvalues. For n odd, steady-states exist for a narrow range of velocities, there are two fixed points for each V, and the eigenvalues of the Jacobian evaluated at the two fixed points have either all negative real parts (upper branch, solid line) or all positive real parts (lower branch, dashed line).

3. KMC Models.

3.1. 2+1 KMC Model.

We employ a standard 2+1 (2D surface with growth in the third dimension) kinetic Monte Carlo (KMC) model which simulates cube-on-cube atomistic growth of surfaces with only nearest neighbor interactions considered. The state of the surface is described by assigning an integer height $h(x, y)$ on a square grid of dimensions $M \times N$; atom desorption is not included. We utilize an in-plane lateral nearest neighbor bond counting model [4] where adatoms hop (diffuse) to neighboring sites with rates given by

$$R = K(T) \exp(-\Delta E/(k_B T))$$

and the diffusion energy barrier ΔE for each surface atom (adatom) is calculated by

$$\Delta E = E_s + nE_n,$$

where E_s is a substrate contribution to the energy barrier present at every lattice location and E_n is a contribution from each of the lateral nearest neighbors, the

number of which can vary from one to four. The energy barriers ΔE vary based on the current surface morphology. The prefactor $K(T)$ is the hopping attempt frequency, typically on the order of $10^{11} - 10^{13}$ attempts/second. Thus, if an atom has an in-plane neighboring atom, it is more tightly bound and it is therefore less probable that a hopping event will occur.

Following Schulze [9], the present model differs from typical 2+1 KMC models of atomistic growth in two ways. First, we implement a substrate pulling velocity V which requires us to shift the substrate in the pulling direction relative to the fixed deposition zone. Second, instead of imposing periodic boundary conditions in both the x and y directions, we enforce the equilibrium condition (3) in the x direction and periodic boundary conditions in the y direction. More specifically, adatoms hopping out of the deposition zone in the x direction vanish, but are replaced at the constant rate of $D\rho_e/4$ atoms per site per unit of time. Ideally, this boundary condition, which is meant to model the state of the film outside the deposition zone, would be enforced in the far-field, but this would slow the simulations by requiring a larger computational domain in the x direction and complicate somewhat the analysis presented in the previous section.

Fig. 7(a) illustrates step edge contours for a representative step profile obtained by running a 2+1 KMC simulation undergoing 500 ML of deposition. In this snapshot, PSP is evident. One can also see a small bit of curvature to the step edge profiles, the presence of which presents a difficulty in obtaining terrace widths for comparison to the terrace widths obtained with a 1-D BCF model. Fig. 7(b) illustrates step edge contours for a representative step profile obtained by running a 2+1 KMC simulation undergoing 500 ML of deposition. Running at a velocity of $V = 11.0$ sites/sec, 1-D BCF theory predicts that there should be a stable 14 step PSP. However, 2+1 KMC produces a stable 13 step pattern where the last two steps are bunched together, almost stacked on top of each other.

In order to allow for comparison of 2+1 KMC results with a 1-D BCF model we proceed in the following manner. Consider an n-step simulation which is run with a constant pulling velocity V for a long enough time to allow for any transients to dissipate. We sample K times during the run after the transient period and obtain height profiles across the domain (i.e., $h_k(x,y)$, $k = 1, \ldots, K$.) One can then obtain effective terrace widths by calculating the level set area for each integer height h and divide by the constant width of the domain to obtain $\{w_{ik}\}_{i=0}^{n}$, the set of terrace widths at sample time t_k. We then average over space and time the alternating interior terrace widths to obtain

$$\bar{\delta_0} = \begin{cases} \dfrac{1}{K}\displaystyle\sum_{k=1}^{K} \frac{2}{n-1} \sum_{i=0}^{\frac{n-1}{2}-1} w_{2i+1,k}, & n \text{ odd} \\ \dfrac{1}{K}\displaystyle\sum_{k=1}^{K} \frac{2}{n} \sum_{i=0}^{\frac{n}{2}-1} w_{2i+1,k}, & n \text{ even.} \end{cases} \tag{31}$$

Fig. 8 illustrates 2+1 KMC $\bar{\delta_0}$ calculations compared with δ_0 calculations for 1-D BCF steady-states. In these runs, $F = 0.5ML/s$ and $L = 165$. After 500 seconds of simulation time running at a fixed velocity V, V is incremented by $\Delta V = 0.05$. As one can see, while there is agreement in general with the slope of the 2+1 KMC data when compared to the 1-D BCF calculations, there is not real good agreement with $\delta_0(V)$ as determined by the two different models.

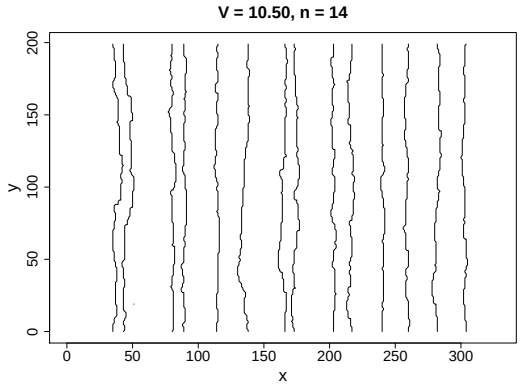

(a) 14 Step, PSP

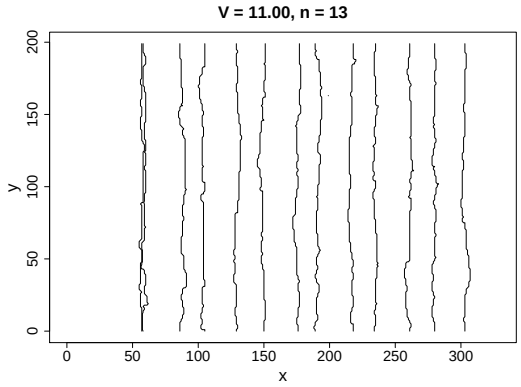

(b) 13 Step, No PSP

FIGURE 7. 2+1 KMC step edge contours (plan view): (a) shows a snapshot of the edge contours after 1000 seconds of simulation time for $F = 0.5$ ML/sec, $n = 14$, and $V = 10.5$ sites/sec, exhibiting a pairwise step pattern. (b) shows a snapshot of the edge contours after 1000 seconds of simulation time for $F = 0.5$ ML/sec, $n = 13$, and $V = 11.0$ sites/sec, which does not exhibit a pairwise step pattern. The 13 step pattern illustrated here is stable in the 2+1 KMC simulations, however 1-D BCF theory predicts that there should exist a PSP for 14 steps.

There are several factors present in the KMC simulations that are absent from the BCF model as formulated here, any of which one might suspect is contributing to the differences outlined above: two dimensional effects such as kinks and step curvature; adatom interactions (including island nucleation); random fluctuations; other time dependent effects, such as systematic oscillations; and adatom detachment from step edges. As the modified simulations presented below will demonstrate, step detachment appears to be the dominant source of disagreement. It is also clear, however, that island formation would invalidate the BCF analysis and steps were taken to avoid this regime in the KMC simulations. It is well known, for example, that when the terrace width is much larger than the mean diffusion

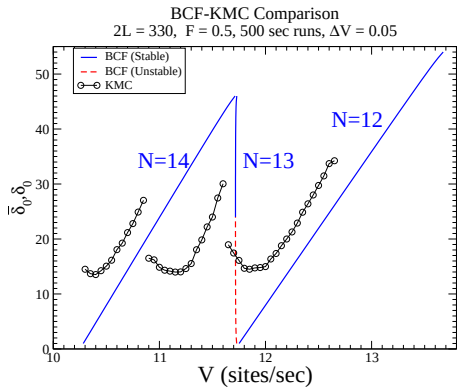

FIGURE 8. Comparison between KMC simulations ($\bar{\delta_0}$) and 1-D BCF (δ_0) steady state predictions. Each data point represents δ_0 averages running at a fixed velocity V for 500 seconds of simulation time, after which V is incremented by $\Delta V = 0.05$ and a new set of averages are taken. Note that 2+1 KMC is not in agreement with 1-D BCF steady state predictions over the velocity range simulated.

length of adatoms on a flat surface, islands will form. To keep island nucleation as low as possible we were restricted to cases with relatively small terrace widths. Utilizing a small E_n also helps, as this increases detachment rates and thus reduces nucleation by breaking up small clusters. Finally, a lower flux F also reduces nucleation, but at the cost of considerably increased simulation time. The various effects noted above are not, however, independent. The reduced terrace widths needed to avoid nucleation, for example, enhance the effects of random fluctuations leading to step collisions with each other and with the boundaries.

3.2. **1-D AAKMC Model.** In order to generate KMC data consistent with the limitations of the continuum model, we target the issues identified in the previous section. To achieve this goal, we have implemented a $1+1$ dimensional KMC model that treats adatom diffusion as a non-interacting random walk on a flat terrace. The noninteracting feature is especially important for a one dimensional surface, as adatoms would interfere with one another at a greatly increased rate. The steps move forward only when an adatom lands in front of the edge (attachment). Steps can move backward for rare events dictated by an independently controlled detachment rate. This makes controlling detachment easier than in the standard KMC simulations presented above, where detachment is dominated by the hopping rate for a singly coordinated atom. If this rate is reduced, it will reduce the dimer break-up rate, greatly enhancing nucleation. Thus, an alternative to the modified approach we present now would be to make a non-nearest neighbor KMC that is able to distinguish between detachment from a step and dimer break-up. We adopted non-interacting random walks instead, because it also allows for 1+1-dimensional simulations, eliminating possible step curvature effects and does not include nucleation. The latter removes the requirement of working with short terrace widths. The modified model remains time-dependent with random fluctuations. Indeed, the fluctuations of the step positions are greatly enhanced without the averaging influence of the second surface dimension. As a result, we find that

we actually need to greatly increase terrace widths to achieve meaningful average step positions. (This explains why the results for the modified KMC simulations are for a wide terrace regime, while the results for the conventional scheme were for a narrow terrace regime; efforts to match the parameters fail for the reasons just noted.) This type of simulation has been applied previously (see [11]), where it was referred to as adatom KMC (AAKMC).

Figures 9 illustrate AAKMC $\bar{\delta_0}$ calculations compared with δ_0 calculations for BCF steady-states. The AAKMC model used to calculate data used in Fig. 9(a) includes adatom detachment, while the AAKMC model used to calculate data used in Fig. 9(b) does not model adatom detachment. In all of these runs, $F = 0.25ML/s$ and $L = 3000$, and each velocity was run for 500 simulation seconds. One can clearly

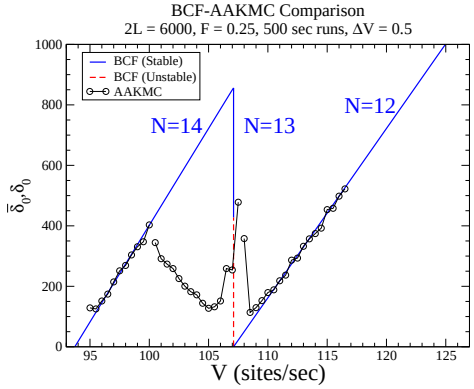

(a) 1-D AAKMC (with adatom detachment) $\bar{\delta_0}$, 1-D BCF δ_0

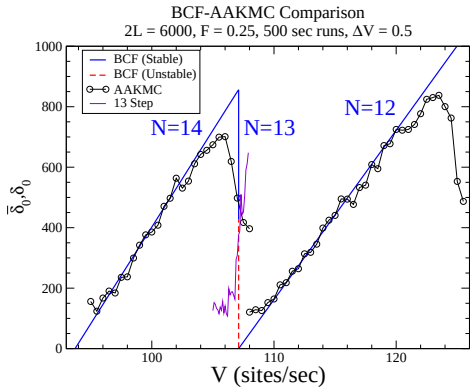

(b) 1-D AAKMC (without adatom detachment) $\bar{\delta_0}$, 1-D BCF δ_0

FIGURE 9. These figures illustrate the different character of 1-D AAKMC when adatom detachment is (a) included and (b) excluded from the simulations. Note that the domain width is large ($L = 3000$) and that excellent agreement between the two models is obtained for the case without adatom detachment. Note that 1-D AAKMC with adatom detachment provides excellent agreement for N even over approximately half of the range predicted by 1-D BCF.

see that PSP is present in the 1-D AAKMC model and agrees well with what is predicted by the BCF approximation, including the very narrow range of velocities V for n odd.

4. **Summary.** The processing scenario considered in this paper differs from that typically considered in the epitaxy literature in that the film is moving relative to the deposition apparatus. We have shown that this can result in important boundary effects that are not captured by the helical boundary conditions—where the lowest step in the train reconnects with the highest—typically imposed in the direction of growth. In particular, the mean-field model reveals novel steady-state solutions with an alternating step spacing that depends on the processing speed V. With the number of steps n even, these steady states are neutrally stable while for n odd, two steady-states coexist over a very narrow range of velocities, with one stable and one unstable.

While the mean-field model gives important insight into this pattern formation, it was found to give only partial agreement with standard KMC simulations. In order to narrow the range of causes of the poor quantitative agreement between the two models, we used a modified 1+1 dimensional KMC with noninteracting adatoms and controllable step detachment rates. It was found that the modified simulations agreed well with the continuum theory when detachment was disabled, and agreed qualitatively with the standard KMC results when detachment was present. It would be interesting for future work to address this apparent shortcoming of the mean field model, perhaps by including an "edge atom" density field, as in the work of E and Yip [7].

REFERENCES

[1] W. K. Burton, N. Cabrera, and F. C. Frank. The growth of crystals and the equilibrium structure of their surfaces. *Phil. Trans. Roy. Soc.*, 243(866):299–358, 1951.

[2] G. S. Bales and A. Zangwill. Morphological instability of a terrace edge during step-flow growth. *Phys. Rev. B*, 41:5500, 1990.

[3] X. Cui, F. A. List, D. M. Kroeger, A. Goyal, D. F. Lee, J. Mathias, E. D. Specht, P. M. Martin, R. Feenstra, D. T. Verebelyi, D. K. Christen, and M. Paranthaman. Reel-to-reel continuous deposition of epitaxial CeO_2 buffer layers on biaxially textured Ni tapes by electron beam evaporation. *IEEE Trans. Appl. Supercond.*, 9(2):1967–1970, June 1999.

[4] Shaun Clarke and Dimitri D. Vvedensky. Growth kinetics and step density in reflection high-energy electron diffraction during molecular-beam epitaxy. *J. Appl. Phys.*, 63(7):2272–2283, 1988.

[5] S. Donet, F. Weiss, P. Chaudouet, S. Beauquis, A. Abrutis, H. C. Freyhardt, A. Usokin, D. Selbmann, J. Eickemeyer, C. Jimenez, C. E. Bruzek, and J. M. Saugrain. Reel-to-reel MOCVD for YBCO coated conductor. *IEEE Trans. Appl. Supercond.*, 13(2):2524, 2003.

[6] G. Ehrlich and F. G. Hudda. Atomic view of surface diffusion: tungsten on tungsten. *J. Chem. Phys.*, 44:1039, 1966.

[7] Weinan E and Nung Kwan Yip. Continuum theory of expitaxial crystal growth. *I. J. Statist. Phys.*, 104:211–253, 2001.

[8] R. L. Schwoebel. Step motion on crystal surfaces, II. *J. Appl. Phys.*, 40(2):614–618, 1968.

[9] Tim P. Schulze. Morphological instability during directional epitaxy. *J. Crystal Growth*, 295:188–201, 2006.

[10] R. L. Schwoebel and Edward J. Shipsey. Step motion on crystal surfaces. *J. Appl. Phys.*, 37(10):3682–3686, 1966.

[11] T. P. Schulze, P. Smereka, and Weinan E. Coupling Kinetic Monte-Carlo and continuum models with application to epitaxial growth. *J. Comp. Phys.*, 189:197–211, 2003.

[12] O. Stadel, J. Schmidt, G. Wahl, F. Weiss, D. Selbmann, J. Eickemeyer, O. Yu. Gorbenko, A. R. Kaul, and C. Jimenez. Continuous YBCO deposition by MOCVD for coated conductors. *Physica C*, 372–376:751–754, 2002.

Received xxxxxx 2008; revised yyyyy 2008.

E-mail address: msaum@math.utk.edu
E-mail address: schulze@math.utk.edu